# Structural evolution in Ti-Cu-Ni metallic glasses during heating

P. Gargarella, S. Pauly, M. Stoica, G. Vaughan, C. R. M. Afonso, U. Kuehn, J. Eckert

# Structural evolution in Ti-Cu-Ni metallic glasses during heating

P. Gargarella, S. Pauly, M. Stoica, G. Vaughan, C. R. M. Afonso, U. Kühn, and J. Eckert

Citation: APL Materials **3**, 016101 (2015); doi: 10.1063/1.4905287
View online: http://dx.doi.org/10.1063/1.4905287
View Table of Contents: http://scitation.aip.org/content/aip/journal/aplmater/3/1?ver=pdfcov
Published by the AIP Publishing

APL MATERIALS **3**, 016101 (2015)

# Structural evolution in Ti-Cu-Ni metallic glasses during heating

P. Gargarella,[1,2,a] S. Pauly,[1] M. Stoica,[1] G. Vaughan,[3] C. R. M. Afonso,[2] U. Kühn,[1] and J. Eckert[1,4]
[1]*IFW Dresden, Institut für Komplexe Materialien, Helmholtzstraße 20, D-01069 Dresden, Germany*
[2]*Departamento de Engenharia de Materiais, Universidade Federal de São Carlos, Rodovia Washington Luiz, Km 235, 13565-905 São Carlos, São Paulo, Brazil*
[3]*European Synchrotron Radiation Facilities, BP 220, 38043 Grenoble, France*
[4]*Institut für Werkstoffwissenschaft, Technische Universität Dresden, D-01062 Dresden, Germany*

(Received 16 October 2014; accepted 16 December 2014; published online 5 January 2015)

The structural evolution of $Ti_{50}Cu_{43}Ni_7$ and $Ti_{55}Cu_{35}Ni_{10}$ metallic glasses during heating was investigated by *in-situ* synchrotron X-ray diffraction. The width of the most intense diffraction maximum of the glassy phase decreases slightly during relaxation below the glass transition temperature. Significant structural changes only occur above the glass transition manifesting in a change in the respective peak positions. At even higher temperatures, nanocrystals of the shape memory B2-Ti(Cu,Ni) phase precipitate, and their small size hampers the occurrence of a martensitic transformation.  [http://dx.doi.org/10.1063/1.4905287]

Ti-Ni-Cu system is well known for the formation of several shape memory alloys (SMAs).[1] These alloys have the intrinsic ability to recover their initial shape after plastic deformation of the low-temperature phase by a reverse martensitic transformation (MT), which occurs upon heating to a critical temperature.[1] Cu-rich Ti-Cu-Ni SMAs exhibit a smaller temperature and stress hysteresis when compared with other TiNi-based SMAs,[1] which make them potential candidates for actuator applications. Moreover, the substitution of Ni by Cu decreases the costs of such SMAs. The cubic high-temperature phase B2-Ti(Cu,Ni) forms in these alloys in the range of $Ti_{50}(Cu_xNi_{50-x})$ $(0 < x < 31)$[1] and transforms directly to the orthorhombic B19 phase around 320 K with the Cu addition.[1] Also other phases than the shape memory B2-Ti(Cu,Ni) can precipitate in these Cu-rich alloys, i.e., TiCu and $Ti_2Cu$,[1] which leads to an embrittlement, reduces the shape recovery, and limits their use.[2] Rapid solidification can hamper the formation of these phases due to kinetic constraints and thus extends the composition range in which the B2-Ti(Cu,Ni) phase forms.[3] At sufficiently high cooling rates, even Ti-Cu-Ni metallic glasses can be obtained by completely suppressing the formation of any crystalline phase.[4] Several Ti-Cu-Ni-based bulk metallic glasses have been already reported but no systematic studies have been conducted to identify their phase formation during crystallization.

Moreover, it is important to understand how the characteristics of the MT are affected by the volume fraction of second crystalline phases around or inside the B2 crystals.[5,6] These precipitates generate elastic strain fields, which interfere with the MT of the shape memory phase, changing the start transformation temperature[6] or the number of transformation steps.[5] The size of the shape memory crystals also influences the MT since grain boundaries hinder the growth of the martensite and impede its autocatalytic nucleation, which is triggered by stresses that arise during its growth.[7] The transformation can be even suppressed for small grain sizes (around 50 nm for TiNi-based alloys)[8] because the stresses required increase with decreasing crystal size.[8]

[a]Author to whom correspondence should be addressed. Electronic mail: piter@ufscar.br

 

The aim of the present work is to investigate the structural evolution of two Ti-Cu-Ni metallic glasses during heating. Structural modifications during relaxation, glass transition, and crystallization are studied using *in-situ* high-energy synchrotron X-ray diffraction. The phase formation during crystallization is moreover associated with their shape memory behaviour.

Ingots of the alloys $Ti_{50}Cu_{43}Ni_7$ and $Ti_{55}Cu_{35}Ni_{10}$ were produced by arc-melting elements with high purity (more than 99.5%). They were repeatedly arc-melted in a Ti-gettered argon atmosphere to ensure complete melting and compositional homogeneity. Ribbons were produced by means of a single-roller melt-spinner with a tangential wheel speed of 42 m/s under argon atmosphere. *In-situ* crystallization studies were performed at the beam line ID11 (European Synchrotron Radiation Facility in Grenoble, France) with high-energy synchrotron radiation of 99.15 keV ($\lambda$ = 0.01249 nm) and a beam size of 50 $\mu m^2$. Slices of a melt-spun ribbon were put inside a 1 mm diameter quartz capillary and then heated at 30 K $min^{-1}$ using a computer-controlled Linkam THMS 600 furnace. XRD patterns were collected in transmission mode every 13 K during heating (acquisition time of 25 s) using a two-dimensional charge-coupled detector FRELON 2k16. A continuous Ar flow was supplied to the sample during the experiments, and the distance between the samples and detector was 272 mm. A $LaB_6$ standard was used to calibrate the sample-to-detector distance, and the background intensity was subtracted directly from the two-dimensional XRD patterns. The result was then integrated to the Q-space using the FIT2D program.[9]

The thermal stability of the ribbons was examined by differential scanning calorimetry (DSC) using a Perkin-Elmer Diamond DSC also at heating rate of 30 K/min. Annealing experiments were also performed in a calorimeter at temperatures between the glass transition and crystallization (693 K and 700 K for the $Ti_{50}Cu_{43}Ni_7$ and $Ti_{55}Cu_{35}Ni_{10}$ ribbons, respectively). These samples were further analysed by means of a STOE STADI P X-ray diffractometer with a Mo-$K_{\alpha 1}$ radiation ($\lambda$ = 0.07093 nm) in transmission mode. The microstructure of the crystallized samples was investigated by scanning electron microscopy (SEM) using a SEM-FEG Gemini 1530, and the composition of the different phases was determined by energy-dispersive X-ray (EDX) analysis using a Bruker Xflash 4010 spectrometer. Further microstructural investigations were conducted in a TECNAI G2F20 transmission electron microscope (TEM). The TEM samples were thinned manually and then made electron-transparent by ion-milling using a Gatan 691 Precision Ion Polishing System with a liquid-nitrogen cooling system.

Three events can be seen during continuous heating of the glassy $Ti_{50}Cu_{43}Ni_7$ ribbon (Figure 1(a)). A broad and shallow exothermic peak precedes the glass transition at 681 ± 2 K ($T_g$) (inset Figure 1(a)). As a result of the relatively high cooling rate during melt-spinning, the glassy structure exhibits local heterogeneities with regions of lower and higher density than the average.[10] This structure relaxes during heating, which releases heat and causes the observed exothermic peak. This structural relaxation starts at 476 ± 2 K ($T_r$) and it is followed by the glass transition during which the metallic glass transforms into a supercooled liquid with high viscosity. The supercooled

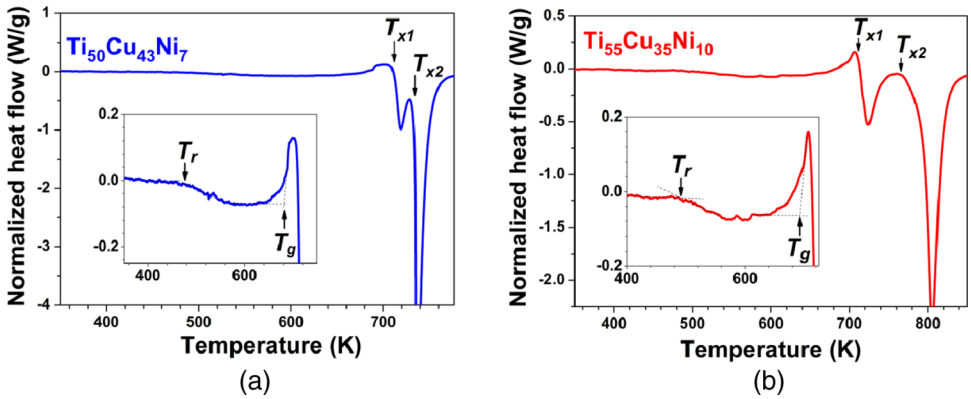


FIG. 1. DSC results for the as-cast (a) $Ti_{50}Cu_{43}Ni_7$ and (b) $Ti_{55}Cu_{35}Ni_{10}$ ribbons at heating rate of 30 K/min. $T_{xi}$ marks the onset of crystallization and $T_r$ the onset of structural relaxation.

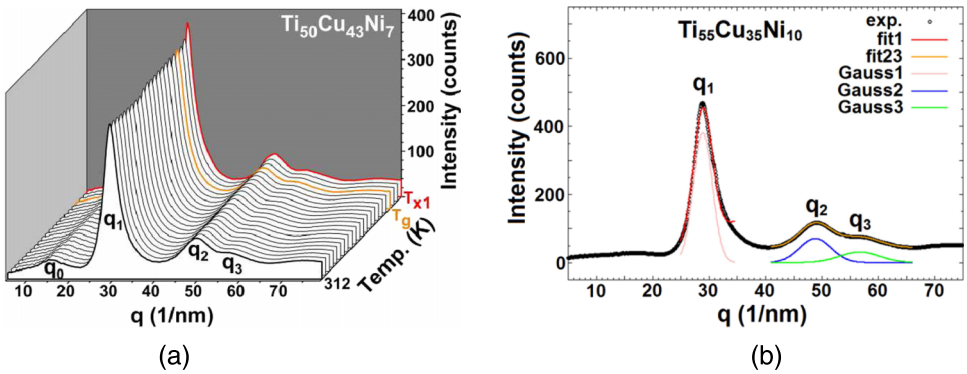


FIG. 2. High-energy XRD patterns of the (a) $Ti_{50}Cu_{43}Ni_7$ ribbon taken at different temperatures during heating ($T_g$ = 681 and $T_{x1}$ = 711 K) at 30 K/min and (b) of the $Ti_{55}Cu_{35}Ni_{10}$ ribbon taken at room temperature. A fitting (denoted fit1 and fit23) was carried out in order to determine the position, intensity, and width of the broad peaks of the glass observed around q = 29, 49, and 57.5 $nm^{-1}$ ($q_1$, $q_2$, and $q_3$, respectively, in (a) and (b)).

liquid eventually crystallizes in two (exothermic) steps at 711 ± 2 K and at 734 ± 2 K. The glassy $Ti_{55}Cu_{35}Ni_{10}$ ribbon shows a similar thermal behaviour like $Ti_{50}Cu_{43}Ni_7$ (Figure 1(b)). A broad exothermic relaxation peak is observed starting at 498 ± 2 K and is followed by the glass transition at 691 ± 2 K (inset Figure 1(b)). Two exothermic crystallization peaks are seen at 710 ± 2 K and around 766 ± 2 K. The second crystallization peak is slightly asymmetric and seems to result from the overlapping of two peaks.

Both the events, which occur during relaxation and the crystallization processes, were investigated in more details by *in-situ* high-energy synchrotron radiation and they will be discussed in the following. Figure 2(a) shows high-energy X-ray diffraction patterns of the $Ti_{50}Cu_{43}Ni_7$ ribbon taken during heating. Four diffuse peaks ($q_0$ to $q_3$ in Figure 2(a)) are observed at 312 K. The first peak at 15 $nm^{-1}$ (pre-peak) is related to the Linkam hot stage used in the experiment to heat the samples (the peak position and intensity do not change with increasing temperature). The second, third, and fourth diffuse peaks stem from the actual sample and they are characteristic of a fully amorphous structure. A similar pattern was obtained for the $Ti_{55}Cu_{35}Ni_{10}$ ribbon, also exhibiting these three broad peaks ($q_1$ to $q_3$ in Figure 2(b)). The pre-peak still occurs for this sample (not indicated in Figure 2(b)) but with a much lower intensity. The position, intensity, and the full width at half maximum (FWHM) of each diffuse peak were obtained by fitting the experimental curves with the analytical function

$$F(x) = Ae^{\left(-\log(2)\left(\frac{(x-Q)}{W}\right)^2\right)} + b_0 + b_1 x, \quad (1)$$

where $A$ is the amplitude, $2W$ is the FWHM, $Q$ is the position of the peak maximum, and $b_0$ and $b_1$ are the constants describing the background. A good fitting was obtained using this function as exemplified in Figure 2(b).

The position and FWHM of each diffuse peak for these samples are recorded as a function of temperature, and the results are summarized in Figures 3(a) and 3(b). The position of the most intense peak ($q_1$) decreases linearly with increasing temperature up to the glass transition for both compositions. In the reciprocal space, a decrease in the peak position results from the increase in the interatomic distance (thermal expansion). No changes are observed in this linear fashion after the beginning of the structural relaxation at $T_r$. In contrast, the FWHM first slightly increases and then becomes smaller after structural relaxation, which reflects a higher structural ordering after beginning of the relaxation process.

A similar trend as described above was found for the position and width of the second most intense peak at around 49 $nm^{-1}$ ($q_2$, Figures 2(a) and 2(b)). The ratio between the position of the second most and the most intense peaks around $q_1$ = 29 $nm^{-1}$ and $q_2$ = 49 $nm^{-1}$ ($q_2/q_1$) are also shown in Figures 3(a) and 3(b) for $Ti_{50}Cu_{43}Ni_7$ and $Ti_{55}Cu_{35}Ni_{10}$, respectively. One can see that the ratio is constant below the glass transition temperature but changes abruptly for higher temperatures, which

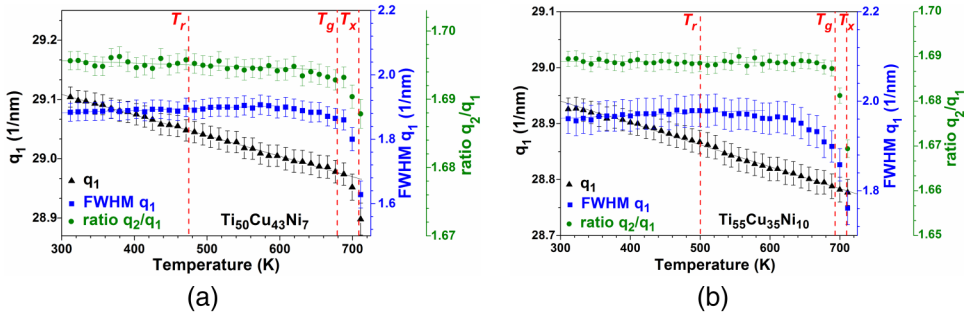


FIG. 3. (a) and (b) Correlation between temperature, the position ($q_1$), and FWHM of the most intense diffraction peak (at $q_1$, Figures 2(a) and 2(b)) and ratio between the position of this peak and the second most intense ($q_2/q_1$) for the glassy (a) $Ti_{50}Cu_{43}Ni_7$ and (b) $Ti_{55}Cu_{35}Ni_{10}$ ribbons. The temperatures onset of relaxation $T_r$, glass transition $T_g$, and crystallization $T_x$ obtained from the DSC measurements are indicated.

is a clear indication of structural changes in the supercooled liquid state.[11] This demonstrates that between the beginning of the relaxation process given by $T_r$ and the glass transition temperature $T_g$, the dominant mechanism of structural changes is the thermal expansion, by which atomic bonds are stretched in a similar fashion for the different shells in the atomic clusters.[12] Although the relaxation already starts to occur as observed by DSC (Figure 1), it does not significantly affect the atomic configuration at this temperature range. Above the glass transition, there is a considerable structural change in the sense that the short-range order behaves differently than the medium-range order. The higher atomic mobility accelerates the relaxation process, which becomes the dominant mechanism of structural change, and the material relaxes towards a state with lower free energy.

The change in the position of peak $q_1$ can then be used to calculate the thermal expansion coefficient. A linear ratio means that the Ehrenfest equation is satisfied,[11,13] and an approximated value of the volumetric thermal expansion coefficient, $\alpha$, can be obtained by the relation[13]

$$\left(\frac{q_1(T_0)}{q_1(T)}\right)^3 = \frac{V(T)}{V(T_0)} = 1 + \alpha(T - T_0), \tag{2}$$

where $q_1$ is the peak position, $V$ is the reduced mean atomic volume, $T$ is the temperature, and $T_0$ is the reference temperature (311 K in this study). A volumetric thermal expansion coefficient $\alpha$ of $(3.66 \pm 0.05) \times 10^{-5}$ and $(4.08 \pm 0.06) \times 10^{-5}$ $K^{-1}$ was obtained for $Ti_{50}Cu_{43}Ni_7$ and $Ti_{55}Cu_{35}Ni_{10}$, respectively, by plotting $(q_1(T_0)/q_1(T))^3$ versus temperature (not shown here). These values correspond to a linear thermal expansion coefficient, $\alpha_l(\alpha = 3\alpha_l)$ of $(1.22 \pm 0.02) \times 10^{-5}$ and $(1.36 \pm 0.02) \times 10^{-5}$ $K^{-1}$, which are very close to the value measured for a $Ti_{50}Cu_{43}Ni_7$ alloy ($1.20 \times 10^{-5}$ $K^{-1}$) by dilatometry.[14]

Selected diffraction patterns collected during heating of the $Ti_{50}Cu_{43}Ni_7$ glassy ribbon are shown in Figure 4(a). Crystallization starts at 711 K ($T_{x1}$) with the precipitation of the cubic B2-Ti(Cu,Ni) followed by formation of the tetragonal γ-TiCu phase at 721 K ($T_{x2}$). These transformation temperature values are similar to the ones measured by DSC. The $Ti_{50}Cu_{43}Ni_7$ glass was annealed at 693 K, between $T_g$ and $T_x$ for 120 s in order to precipitate the B2-Ti(Cu,Ni) phase. The microstructure of this sample is shown in the TEM image of Figure 4(b). It consists of small crystals with sizes <10 nm and with irregular morphology, inserted in an amorphous matrix. The selected area electron diffraction pattern (SAED) of this region is shown in the inset of Figure 4(b). Diffuse diffraction rings of the amorphous phase are seen together with thin and weak rings, which can be indexed as the B2-Ti(Cu,Ni) phase. The microstructure of this sample after complete crystallization (not shown here) exhibits very fine equiaxial grains of the γ-TiCu phase surrounded by a very small amount of B2-Ti(Cu,Ni) in the grain boundary with average grain sizes around 200 and <50 nm, respectively.

Figure 5(a) shows selected XRD patterns of the $Ti_{55}Cu_{35}Ni_{10}$ ribbon taken at different temperatures. The first phase precipitates at 711 K and it is a metastable nanocrystalline phase with broad peaks at $q$ = 15, 28.5, and 47.5 $nm^{-1}$ (highlighted by dashed blue circles in Figure 5(a)). These

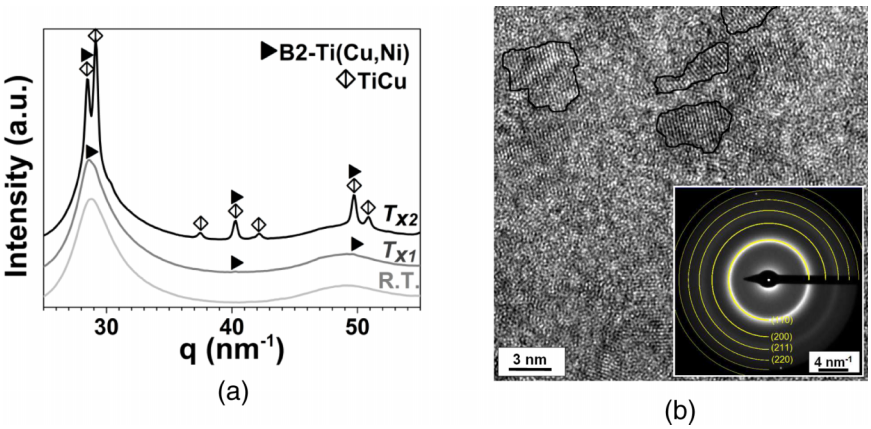


FIG. 4. (a) Selected XRD patterns obtained during heating of the $Ti_{50}Cu_{43}Ni_7$ ribbon. R.T. means room temperature. The values of $T_{x1}$ and $T_{x2}$ are 711 ± 2 and 721 ± 2 K, respectively. (b) High-resolution TEM image of the $Ti_{50}Cu_{43}Ni_7$ ribbon annealed at 693 K (between $T_g$ and $T_x$). The SAED of this region is shown in the inset.

reflections could not be indexed as the expected equilibrium phases B2-Ti(Cu,Ni), $CuTi_2$ phases, and γ-TiCu.[15] Subsequently, the tetragonal γ-TiCu phase precipitates at 756 K followed by the decomposition of the metastable nanocrystalline phase into B2-Ti(Cu,Ni) and tetragonal $CuTi_2$ at 766 K (Figure 5(a)). Only peaks related to the γ-TiCu, B2-Ti(Cu,Ni), and $CuTi_2$ phases are observed at 969 K. These results suggest that the second crystallization peak observed in Figure 5(b) is actually the superposition of two exothermic events related to the precipitation of the γ-TiCu and the decomposition of the metastable nanocrystalline phase into the B2-Ti(Cu,Ni) and $CuTi_2$ phases.

Also a glassy $Ti_{55}Cu_{35}Ni_{10}$ ribbon was annealed at 700 K between the glass transition temperature and the first crystallization event. Figure 5(b) shows a TEM image of the resulting microstructure. Spherical nanocrystalline precipitates with size ~5 nm can be seen homogeneously dispersed in the matrix. This is supposed to be the metastable nanocrystalline phase observed by the *in-situ* XRD experiments (Figure 5(a)). The SAED pattern of this region (inset, Figure 5(b)) shows broad diffraction rings typical of an amorphous structure together with weak but sharp rings, which are probably related to the metastable phase. The bright field TEM image in Fig. 5(c) shows the microstructure of a fully crystalline sample after being heated to 973 K. Crystals with sizes smaller than 50 nm are observed surrounded by a black phase. EDX analyses prove that the black phase is $CuTi_2$, whereas the crystals correspond to the B2-Ti(Cu,Ni) and TiCu as detected by XRD.

Interestingly, no martensitic transformation was observed by DSC for the annealed ribbons of $Ti_{50}Cu_{43}Ni_7$ and $Ti_{55}Cu_{35}Ni_{10}$ in the temperature range between 223 and 473 K. None of the

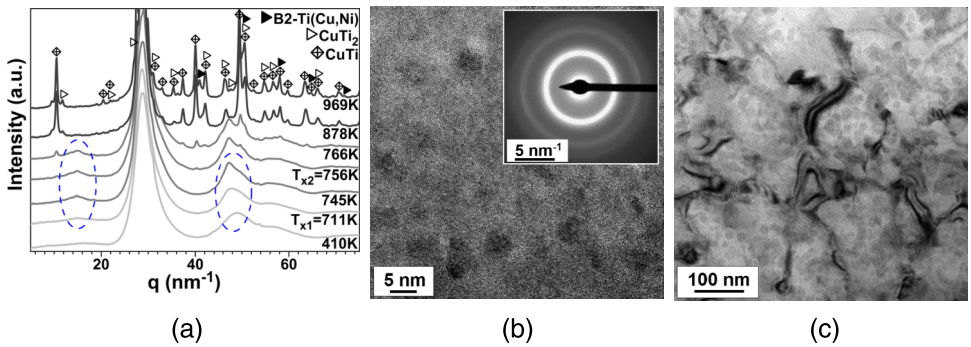


FIG. 5. (a) XRD patterns obtained during heating of the glassy $Ti_{55}Cu_{35}Ni_{10}$ ribbon. The blue dashed circles show peaks of an unknown metastable nanocrystalline phase. (b) High-resolution TEM image of the $Ti_{55}Cu_{35}Ni_{10}$ ribbon annealed at 700 K (between $T_g$ and $T_{x1}$). The SAED of this region is shown in the inset. (c) Bright field TEM images of the ribbon heated up to 973 K until complete crystallization.

partially or fully crystalline ribbons exhibit a thermally induced martensitic transformation.[3] As observed in our previous work,[14] the $Ti_{50}Cu_{43}Ni_7$ alloy shows martensitic transformation around 350 K in samples partially or fully crystalline produced by casting. The B2 crystals in these samples exhibit sizes in the micrometer scale.[14] In contrast, the B2 crystals present in the annealed samples exhibit typical sizes below 50 nm (Figures 4(b) and 5(c)). As discussed by Waitz *et al.*,[7,8] a transformation barrier of strain and interface energy arises, which suppresses the transformation in crystals with sizes smaller than 50 nm. The large amount of grain boundaries in the annealed samples acts as obstacles that hinder the growth of the martensite and its autocatalytic nucleation potency[7] and this explains the absence of transformation in the annealed samples.

To conclude, the structural changes during heating of two Ti-Cu-Ni metallic glasses were monitored by *in-situ* high-energy XRD. During relaxation, the elimination of structural defects is observed by a slight decrease in the FWHM of $q_1$ (Figures 3(a) and 3(b)). Significant structural changes start to occur only after $T_g$ with a significant change in the ratio $q_2/q_1$. The crystallization of the $Ti_{50}Cu_{43}Ni_7$ glassy ribbon occurs with the formation of the B2-TiNi and γ-TiCu phase, respectively, and the crystallization of the $Ti_{55}Cu_{35}Ni_{10}$ alloy occurs in three steps with the formation of a metastable nanoscale phase in the first crystallization process followed by the precipitation of the γ-TiCu phase and the decomposition of the metastable nanocrystalline phase into B2-Ti(Cu,Ni) and $CuTi_2$, respectively. None of the partially or fully crystalline ribbons exhibit a thermally induced martensitic transformation, which is attributed to the small size of the B2-Ti(Cu,Ni) phase (<50 nm).

This work was supported by CNPq and FAPESP, Brazil, and DAAD, Germany. The authors are grateful to B. Bartusch, Dr. L. Giebeler, and D. Lohse for technical assistance.

[1] K. Otsuka and X. Ren, Prog. Mater. Sci. **50**, 511-678 (2005).
[2] H. Rösner, P. Schloßmacher, A. V. Shelyakov, and A. M. Glezer, Scr. Mater. **43**, 871–876 (2000).
[3] P. Gargarella, S. Pauly, K. K. Song, J. Hu, N. S. Barekar, M. S. Khoshkhoo, A. Teresiak, H. Wendrock, U. Kühn, C. Ruffing, E. Kerscher, and J. Eckert, Acta Mater. **61**, 151-162 (2013).
[4] Y. L. Wang and J. Xu, Metall. Mater. Trans. A **39**, 2990-2997 (2008).
[5] T.-h. Nam, J.-h. Lee, G.-b. Cho, and Y.-w. Kim, Mater. Sci. Eng.: A **438-440**, 687-690 (2006).
[6] H. Rösner, P. Schloßmacher, A. V. Shelyakov, and A. M. Glezer, Acta Mater. **49**, 1541-1548 (2001).
[7] T. Waitz, T. Antretter, F. D. Fischer, and H. P. Karnthaler, Mater. Sci. Technol. **24**, 934-940 (2008).
[8] T. Waitz, T. Antretter, F. D. Fischer, N. K. Simha, and H. P. Karnthaler, J. Mech. Phys. Solids **55**, 419-444 (2007).
[9] A. P. Hammersley, S. O. Svensson, M. Hanfland, A. N. Fitch, and D. Hausermann, High Pressure Res. **14**, 235-248 (1996).
[10] T. Egami, J. Alloys Compd. **509**(1), S82–S86 (2011).
[11] N. Mattern, M. Stoica, G. Vaughan, and J. Eckert, Acta Mater. **60**, 517-524 (2012).
[12] H. W. Sheng, W. K. Luo, F. M. Alamgir, J. M. Bai, and E. Ma, Nature **439**, 419-425 (2006).
[13] A. R. Yavari, A. L. Moulec, A. Inoue, N. Nishiyama, N. Lupu, E. Matsubara, W. J. Botta, G. Vaughan, M. D. Michiel, and Å. Kvick, Acta Mater. **53**, 1611-1619 (2005).
[14] P. Gargarella, Ph.D. dissertation (Dresden University of Technology, Dresden, 2014).
[15] G. Cacciamani and J. C. Schuster, "Cu-Ni-Ti(copper-nickel-titanium)," in *SpringerMaterials—The Landolt-Börnstein Database*, edited by G. Effenberg and S. Ilyenko (Springer, 2006).